Macromolecules

ARTICLE

pubs.acs.org/Macromolecules

Combined Main-Chain/Side-Chain Liquid Crystalline Polymer with Main-Chain On the basis of "Jacketing" Effect and Side-Chain Containing Azobenzene Groups

He-Lou Xie,[†,‡] Shao-Jie Wang,[‡] Guan-Qun Zhong,[†] Yi-Xin Liu,[§] Hai-Liang Zhang,[*,†] and Er-Qiang Chen[*,‡]

[†]Key Laboratory of Polymeric Materials and Application Technology of Hunan Province, Key Laboratory of Advanced Functional Polymer Materials of Colleges and Universities of Hunan Province, College of Chemistry, Xiangtan University, Xiangtan 411105, Hunan Province, China

[‡]Beijing National Laboratory for Molecular Sciences, Department of Polymer Science and Engineering and Key Laboratory of Polymer Chemistry and Physics of Ministry of Education, College of Chemistry and Molecular Engineering, Peking University, Beijing 100871, China

[§]State Key Laboratory of Molecular Engineering of Polymers, Department of Macromolecular Science, Fudan University, Shanghai 200433, China

S *Supporting Information*

ABSTRACT: Combining the concept of "flexible spacer" which can bring liquid crystalline (LC) properties to the side-chains and the side-group "jacketing" effect which can result in main-chain with rod-like conformation, we have synthesized a new combined main-chain/side-chain LC polymer based on radical polymerization, poly(2,5-bis{[6-(4-methoxy-4′-oxy-azobenzene)hexyl]oxycarbonyl}styrene) (denoted as P_1) with two azobenzene groups per repeating unit. The chemical structures of P_1 and the corresponding monomer were characterized using various techniques with satisfactory analysis data. The phase structures and transitions of P_1 were investigated using differential scanning calorimetry, polarized optical microscope, and one- and two-dimensional (1D and 2D) wide-angle X-ray diffraction. We identify that P_1 can form a hierarchically ordered structure with double orderings on both the nanometer and subnanometer length scales. Most likely, the thick main-chains of P_1 obtained by "jacketing" the central rigid portion of terephthalate side-chain to the polyethylene backbone construct a 2D centered rectangular scaffold, which is stable until the sample becomes completely isotropic. The packing of side-chains inside the main-chain scaffold undergoes the transitions of smectic B- (SmB-) like ↔ smecitc A (SmA)-like ↔ isotropic. The confinement arising from the scaffold induces the SmB-like packing and enhances the stability of SmA-like structure. The hierarchically ordered structure of P_1 renders a biaxial orientation with the side-chains perpendicular to the main-chains. We compared P_1 with an end-on side-chain LC polymer of poly(4-{[6-(4-methoxy-4′-oxy-azobenzene)hexyl]oxycarbonyl}styrene) (denoted as P_2). P_2 bearing one mesogenic group per repeating unit forms a monolayer SmA phase, with the transition temperature much lower than that of P_1. Upon UV irradiation, in contrast to that P_2 will become isotropic, P_1 can still exhibit LC behavior after the azobenzene groups adopt cis conformation.

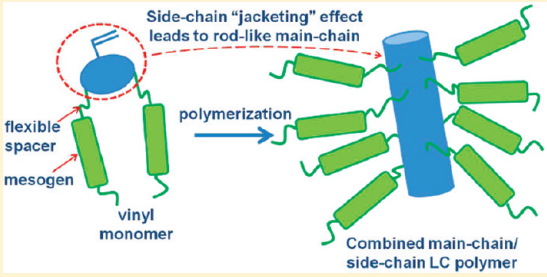

INTRODUCTION

Owing to their anisotropic properties and self-assembling capabilities, liquid crystalline (LC) polymers can be applied in many areas such as engineering plastics and optical and electro-optical devices. Different LC properties and supramolecular structure of LC polymers have immense impacts on their performance as functional materials. Therefore, phase structures and transitions of LC polymers have also been an important subject in fundamental researches.[1−4] In the past decades, numerous endeavors have been paid to rationally design and synthesize polymers with controllable supramolecular structures. For main-chain LC polymer (MCLCP) and side-chain LC polymers (SCLCP), some useful strategies to tailor the LC properties are selecting different mesogenic groups to incorporate into polymers, varying the location of the mesogens, altering the lengths and types of flexible spacers, etc.[5−11] Combination of the chemical features of MCLCP and SCLCP can result in a hybrid structure, which is known as combined main-chain/side-chain LC polymer (MCSCLCP).[12] It is expected that MCSCLCP may have more complex behaviors relative to conventional MCLCPs and SCLCPs, and the interplay between main-chain and side-chain of MCSCLCP may lead to versatility of the LC properties and supramolecular structures.

Received: April 13, 2011
Revised: August 10, 2011
Published: September 08, 2011

Since the first example reported by Ringsdorf et al.,[13,14] quite a few MCSCLCPs have been synthesized and stuided.[15−23] Generally, the method employed to obtain MCSCLCP is condensation polymerization. In this case, the main-chain can either be rigid rod or possess an alternative structure of rod-like mesogenic groups and flexible spacers; and the side-chain is usually composed of mesogenic group linked to the main-chain repeating unit through a flexible spacer. Recently, we suggested a new route to achieve MCSCLCP based on chain polymerization method. The polymer we reported is poly(2,5-bis{[6-(4-butoxy-4′-oxybiphenyl)hexyl]oxycarbonyl}styrene) (PBBHCS), which was synthesized by using free radical polymerization of the corresponding 2-vinylterephthalate monomer.[24] Note that in PBBHCS the central benzene ring of the relatively large terephthalate side-chain is directly attached to every second carbon atom along the polyethylene backbone. In this context, PBBHCS belongs to the catalog of side-on SCLCP and moreover, shares the main feature with mesogen-jacketed LC polymer (MJLCP) at the chemical structure level. During the past years, we have systematically investigated the syntheses and LC behaviors of MJLCP with the "waist" of rod-like mesogenic groups laterally attached to the flexible backbone via a short linkage or a single carbon−carbon bond.[25−27] The absence of flexible spacers leaves the backbone and side-chains of MJLCP fusing together. It is conceivable that the rigid or other bulky side-chains crowdedly placed around the backbone can give a significant "jacketing" effect, forcing the backbone to well extend.[28−37] In this case, the MJLCP chain with sufficiently high molecular weight (MW) looks like a molecular rod as a whole, which can act as the building block of columnar LC (Φ) phases. We have further demonstrated that once the nonmesogenic groups jacketed to the flexible backbone can impose sufficient steric hindrance, the resultant side-chain polymer can also exhibit a rod-like conformation and form a long-range ordered Φ phase, as exemplified by poly[di(alkyl) vinylterephthalate] (PDAVT, with the alkyl ranging from propyl/isopropyl to hexyl).[38] When designing PBBHCS as a MCSCLCP, we have applied the "jacketing" effect.[39] Namely, the rod-like main-chain of PBBHCS is due to the integration of the polyethylene backbone and the central rigid portion of the terephthalate side-chains.

Scheme 1. Schematic Drawing of the Vinyl Monomer Which Can Result in MCSCLCP after Chain Polymerization

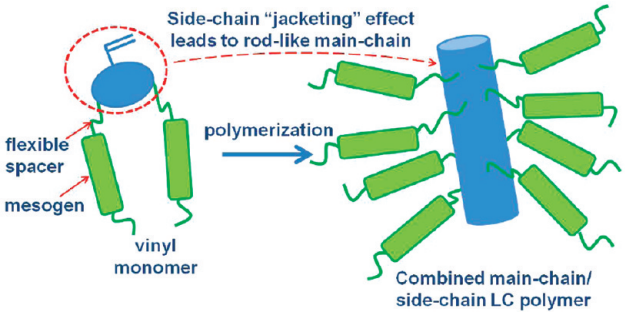

The mesogenic groups of biphenyl are incorporated into PBBHCS at both sides of the side-chain. Following the concept of "flexible spacer", we inserted a flexible spacer of six methylene units between the main-chain and biphenyl group. PBBHCS can exhibit fascinating hierarchical supramolecular structures with double orderings on the nanometer and subnanometer length scales at low temperatures.[39] The main-chains construct a centered rectangular scaffold with two-dimensional (2D) long-range order; and the biphenyl containing side-chains fill inside the scaffold with their axis perpendicular to the main-chain, forming a smectic E- (SmE-) like structure. In this case, PBBHCS possess a biaxial orientation. As illustrated in Scheme 1 using vinyl monomer as an example, we suggest that to obtain MCSCLCP by chain polymerization, the monomer should simultaneously have two different functional components, of which one can offer the "jacketing" effect to the normally flexible or semiflexible backbone and the other with mesogens can form surrounding LC phases.

In the present work, we report the syntheses and phase behaviors of poly(2,5-bis{[6-(4-methoxy-4′-oxy-azobenzene)hexyl]-oxycarbonyl}styrene) (P_1 in Chart 1), of which the chemical structure is similar to PBBHCS. One aim of this work is to demonstrate the generality of the proposed molecular design. We replaced the biphenyl group in PBBHCS by a relatively larger azobenzene moiety, which in the trans conformation is also a typical mesogenic unit. It is well-known that azobenzene containing SCLCPs can form low-ordered LC phases such as nematic (N) and smectic A (SmA).[40−44] The LC behavior can significantly influence the photoresponsive properties of azobenzene moieties.[45−48] In this context, we are also interesting in if P_1 can offer new phase structures to azobenzene side-chains, which might lead to unique properties of photoinduced anisotropy and photochemical phase transition. Mainly on the basis of wide-angle X-ray diffraction (WAXD) results, we find that altering mesogenic group from biphenyl to azobenzene does not eliminate the capability of P_1 as a MCSCLCP to form a possible main-chain scaffold similar to that of PBBHCS. In this paper, we also make a comparison between P_1 and an end-on SCLCP of poly(4-{[6-(4-methoxy-4′-oxy-azobenzene)hexyl]oxycarbonyl}-styrene) (P_2 in Chart 1). Both the P_1 and P_2 share the same mesogenic group. Moreover, P_2 has its chemical structure in the vicinity of polyethylene backbone more or less similar to that of P_1. We find that P_2 forms a common monolayer SmA

Chart 1. Chemical Structures of P_1 and P_2

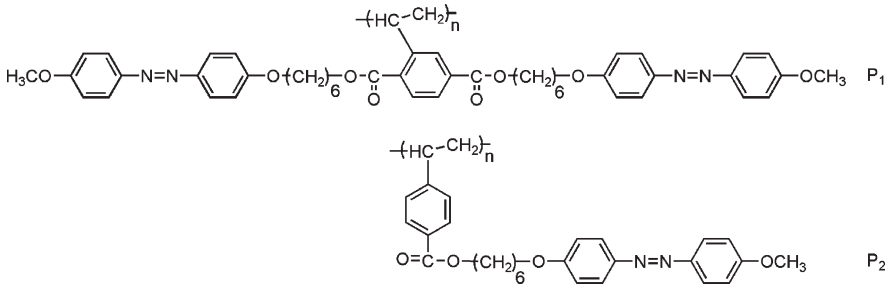

Scheme 2. Synthetic Route of the Monomers (M_1 and M_2) and the Corresponding Polymers (P_1 and P_2)

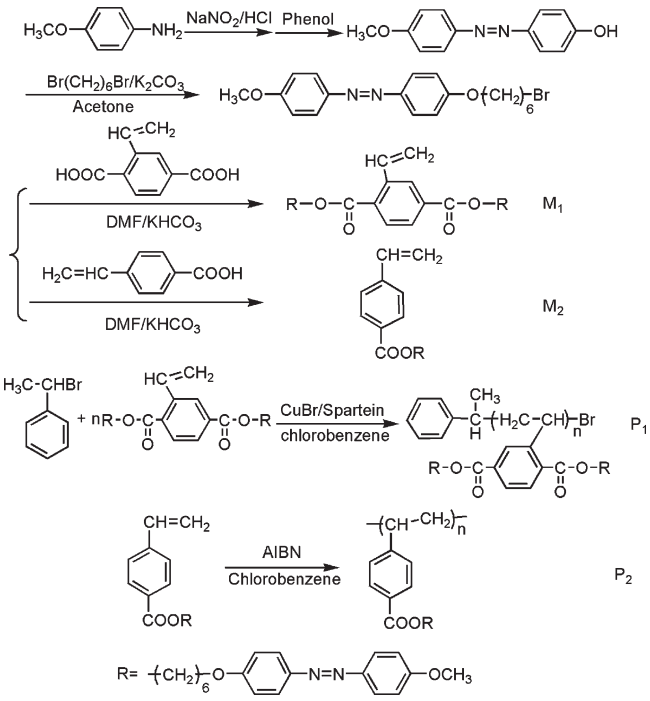

phase at low temperatures[49−52] and its transition temperatures are much lower than that of P_1. We are aware of that the main-chain scaffold of P_1 can in fact impose a significant confinement effect on the side-chain packing, resulting in an unexpected smectic B (SmB)-like structure which is seldom observed in azobenzene containing polymers. We preliminarily examined the phase behaviors of P_1 and P_2 under the UV irradiation. While P_2 can undergo LC-isotropic transition due to the trans−cis isomerization of azobenzene, P_1 renders a schlieren texture which may be attributed to that the rod-like main-chains form a columnar nematic phase (Φ_N).

EXPERIMENTAL SECTION

Synthesis. The synthetic routes of the monomers (M_1 and M_2) and polymers (P_1 and P_2) are shown in Scheme 2. To obtain P_1 with relatively narrow MW distribution, we used the method of atom transfer radical polymerization (ATRP). P_2 was synthesized by conventional solution radical polymerization. The detailed synthesis and characterization of intermediates, monomers, and polymers are shown in the Supporting Information.

Instruments and Measurements. ^{1}H and ^{13}C NMR spectra were recorded on a BRUKER ARX 400 MHz spectrometer at room temperature with $CDCl_3$ or dimethyl sulfoxide-d_6 (DMSO-d_6) as the solvent and TMS as the internal standard. Elemental analysis was carried out with an Elementar Vario EL instrument. The apparent number-average MW (M_n) and MW distribution (M_w/M_n) were measured at 35 °C by a gel permeation chromatography (GPC, WATERS 1515) equipped with three Waters μ-Styragel columns (10^3, 10^4, and 10^5 Å) in series, using THF as the eluent at a flow rate of 1.0 mL/min. The GPC calibration curve was obtained with linear polystyrene as standard. Thermogravimetric analysis (TGA) was performed on a TA-SDT 2960 instrument at a heating rate of 10 °C/min in nitrogen or air atmosphere. Density measurement of the samples was conducted using a flotation technique. We let the sample to equilibrate with a mixture of tetrachloride and petroleum after matching the buoyancy of the sample and the surrounding liquid at room temperature. In this case, the sample was floated freely for an extended period of time. A pycnometer was then filled with the mixture to be weighed.

Differential scanning calorimetry (DSC, PerkinElmer Pyris I) was employed to detect the phase transition behaviors of the samples. The temperature and heat flow were calibrated using benzoic acid and indium. Samples with a typical mass of 3−5 mg were encapsulated in sealed aluminum pans. LC texture of the polymers was examined under polarized optical microscopy (POM, Leica DM-LM-P) coupled with a Mettler-Toledo hot stage (FP82HT) at various temperatures. The POM film samples with thickness of ∼10 μm were casted from THF solution and slowly dried at room temperature. POM images of the film samples exposed to UV radiation (λ = 365 nm) were recorded at 80 °C. One- and two-dimensional (1D and 2D) WAXD experiments were carried out using a Philips X'Pert Pro diffractometer with an X'celerator detector and a Bruker D8 Discover diffractometer in a transmission mode using a GADDS detector, respectively. For both diffractometers, the X-ray sources (Cu Kα) were provided by 3 kW ceramic tubes, and the diffraction peak positions were calibrated with silicon powder ($2\theta > 15°$) and silver behenate ($2\theta < 10°$). The background scattering was recorded and subtracted from the sample patterns. To perform the 2D WAXD experiments with the point-focused X-ray as the incident beam, we prepared the macroscopically oriented samples by mechanical shear at temperatures close to the samples' isotropic temperature.

RESULTS AND DISCUSSION

Synthesis of the Polymers. The monomers of M_1 and M_2 were successfully synthesized through multistep reactions, with their chemical structures confirmed by various characterization techniques. The two monomers could be polymerized readily using radical polymerization method. As shown in Figure 1 of the ^{1}H NMR spectra of M_1 and P_1, the characteristic resonance peaks of the vinyl substituent of monomer at chemical shifts of 7.48−7.41, 5.88−5.83, and 5.54−5.51 ppm (denoted as j, l, and k, respectively) disappear completely after polymerization. Moreover, the chemical shifts of P_1 become quite broad, consistent with the expected polymer structure. We found that both P_1 and P_2 are soluble in common organic solvents such as THF, chloroform, toluene, and chlorobenzene. The thermal stability of P_1 and P_2 was investigated with TGA. For P_1, the temperatures at 5% weight loss were higher than 360 and 300 °C in nitrogen and in air atmosphere, respectively. P_2 is relatively more stable than P_1 upon heating. The molecular characterization results of P_1 and P_2 are summarized in Table 1.

We synthesized P_1 via the ATRP method using CuBr/sparteine as the catalyst and 1-bromoethylbenzene as the initiator. The resultant P_1 samples possess moderately high MWs with relatively narrow MW distribution in good-to-excellent yields (see Table 1). Our GPC experiments showed that with increasing the molar ratio of monomer $\{[M]_o\}$ to initiator $\{[I]_o\}$ ($[M]_o/[I]_o$), the elution time of P_1 samples (P_1-1 to P_1-5) gradually decreases, corresponding to the $M_{n,GPC}$ increasing from 1.21×10^4 to 5.98×10^4 g/mol. All the GPC traces were unimodal (see the Supporting Information). Although the polydispersity increases with increasing MW, it is still lower than the theoretical value of 1.5 for the controlled/"living" free radical polymerization, indicating a good agreement with the rule of ATRP.[53] According to the conversion of monomer and the molar ratio of $[M]_o/[I]_o$, we calculated the theoretical MWs ($M_{n,th}$) of P_1 (see Table 1).[24] The values of $M_{n,th}$ are always slightly higher than that of $M_{n,GPC}$, which may be ascribed to the difference in

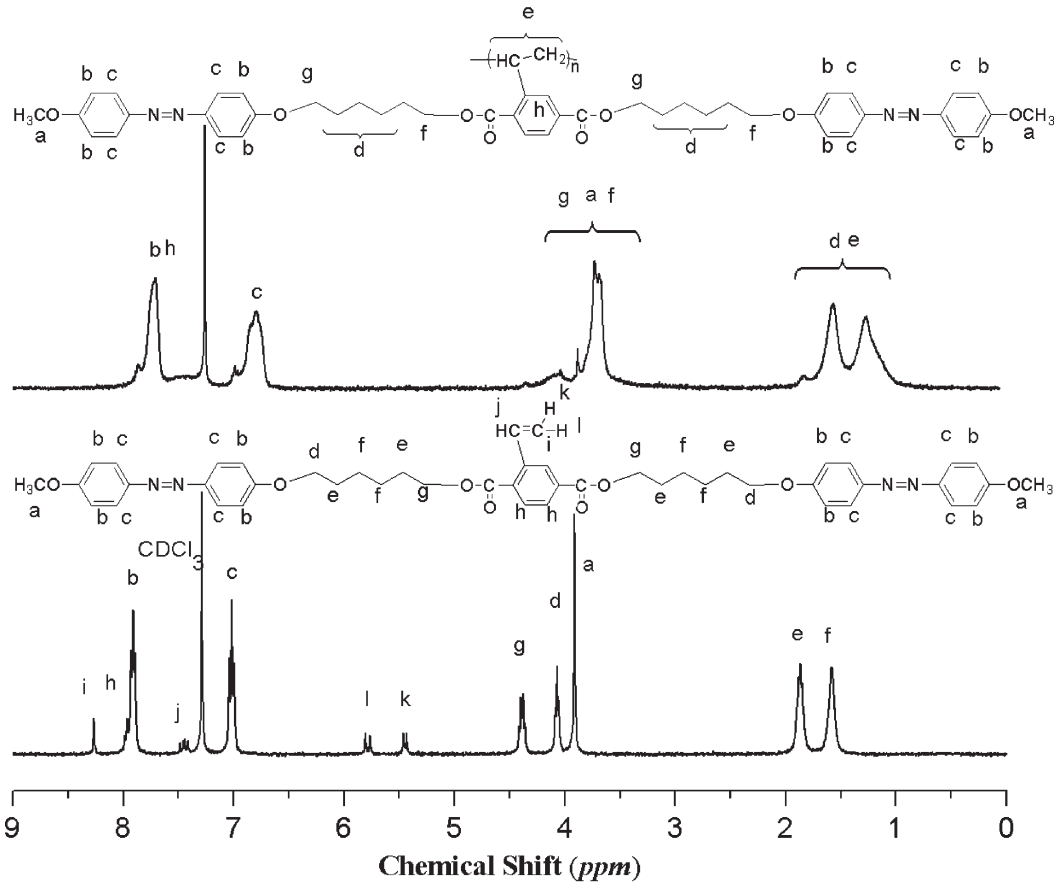

Figure 1. ^{1}H NMR spectra of M_1 (lower panel) and P_1 (upper panel).

Table 1. Molecular Characterization Data of P_1 and P_2

sample	yield[a] (%)	$M_{n,th}$[a] ($\times 10^{-4}$ g/mol)	$M_{n,GPC}$[b] ($\times 10^{-4}$ g/mol)	M_w/M_n[b]	T_d (N_2)[c,d]	T_d (air)[c,d]
P_1-1	60	1.31	1.21	1.16	366	305
P_1-2	65	2.31	2.21	1.15	371	309
P_1-3	80	4.01	3.82	1.21	363	304
P_1-4	90	4.97	4.72	1.26	370	300
P_1-5	90	6.66	5.98	1.47	368	303
P_2	89		3.50	1.95	375	338

[a] Yield and $M_{n,th}$ were calculated according to the method mentioned in ref 24. [b] Obtained from Waters 1515 instrument with the standard of linear polystyrene. [c] The temperature at which 5% weight loss of the sample was reached under nitrogen atmosphere. [d] The temperature at which 5% weight loss of the sample was reached under air atmosphere.

hydrodynamic properties between P_1 and the linear polystyrene standards used in GPC measurements.

Overall Phase Transition Behavior of P_1. The phase transition behavior of P_1 was first examined using DSC experiment. Figure 2 depicts a set of DSC cooling traces of the five P_1 samples with different MWs recorded at a rate of 10 °C/min after the samples' thermal history was erased by heating to the isotropic state, wherein three exothermic peaks are evidenced. These first-order transitions are enantiotropic, which could also be observed in DSC heating scan. The onset temperatures of the three transitions measured from the DSC cooling curves are plotted in Figure 2b as functions of MW. The transition temperatures increase with increasing MW, and the middle one shifts more significantly compared to the other two. Careful examination of the DSC results can reveal the temperature region of glass transition. Note that the baselines of DSC cooling curves before and after the low-temperature transition are obviously deviated. This implies that glass transition of the samples occurred right after the broad transition, and thus the glass transition temperature (T_g) should be of ~80 °C.

At temperatures below the highest transition temperature, P_1 exhibited strong birefringence, and the POM textures clearly indicted the existence of LC phases. The POM samples obtained by THF solution casting usually presented grainy textures composed of tiny LC domains. Upon heating, the texture became slightly different when the samples crossed over the low- and middle-temperature transitions, and the dramatic change of color could be observed accordingly. Figure 3 shows three typical POM images recorded from P_1-4 at 25, 140, and 165 °C, respectively, corresponding to the three LC phases. All five P_1 samples gave similar POM textures and texture evolution with varying temperature. Combining the DSC and POM experimental results together, we consider that the P_1 samples with different MWs share a same phase transition sequence.

The phase transitions could be followed by 1D WAXD thermal experiments. Using P_1-4 as an example, Figure 4 depicts a set of 1D WAXD patterns at various temperatures upon heating after the sample was well annealed at ~85 °C. We found that the diffraction of fresh cast sample was quite weak. Annealing at

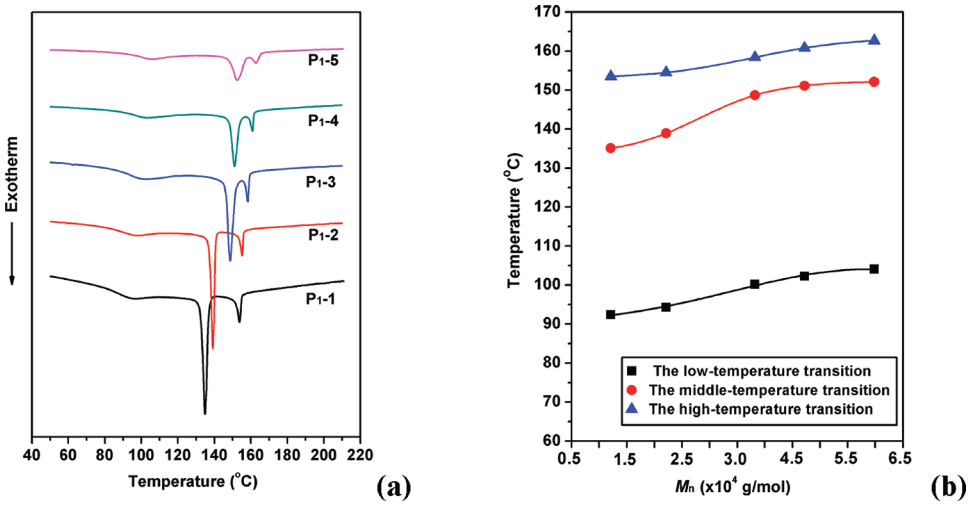

Figure 2. (a) DSC cooling curves of P_1-1 to P_1-5 at a rate of 10 °C/min. (b) MW dependence of the transition temperatures of P_1.

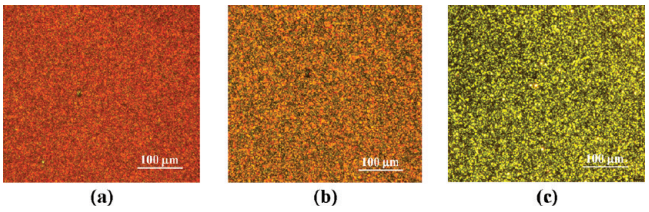

Figure 3. POM images of P_1-4 at (a) 25, (b) 140, and (c) 165 °C.

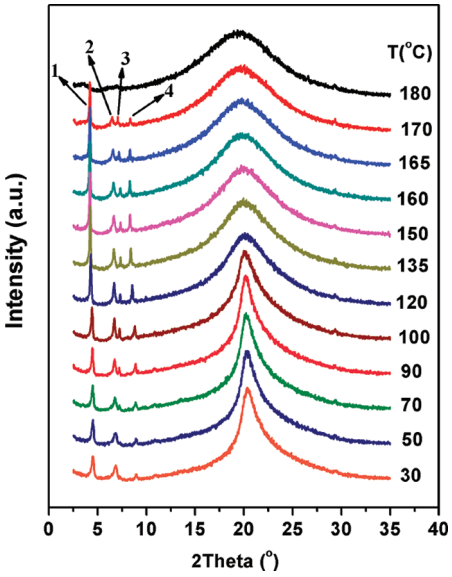

Figure 4. Set of 1D WAXD patterns of P_1-4 recorded during heating process.

temperatures around T_g could substantially increase the diffraction intensity. As shown in Figure 4, the sample renders a single diffraction peaked at 2θ of 20.3° in the high-angle region at low temperatures, which turns into a diffuse scattering halo when the temperature exceeds 110 °C. In the low-angle region, four diffraction peaks (indexed as peak 1, 2, 3, and 4 in Figure 4) can be identified. At below 90 °C, peak 3 is rather weak. This peak increases in intensity with increasing temperature, and its position remains almost unchanged at below 165 °C. As the peaks of 1 and 2 gradually shift toward lower angles, peak 2 and 3 become more separated after 120 °C. When temperature reaches 180 °C, all the low-angle diffractions disappear, indicating that the sample enters an isotropic state. The low- and high-angle diffractions at low temperatures indicate that P_1 possesses two ordered structures on different length scales of nanometer and subnanometer, respectively. This diffraction behavior is similar to that observed from PBBHCS. We consider that the high-angle diffraction at 2θ of 20.3° should be contributed from the packing of azobenzene containing side-chains, and the low-angle diffractions reflect the existence of an ordered structure formed by the main-chains composed of polyethylene backbone and the center rigid portion of side-chain. Since the 1D WAXD patterns lack dimensionality, 2D WAXD experiment was employed to identify the supramolecular structures of P_1.

Phase Structure Identification of P_1. Macroscopically oriented samples for 2D WAXD experiments were obtained by mechanical shear at temperatures slightly below the isotropic temperature. Figure 5a schematically shows the sheared sample with *x*- and *z*-direction the shear direction and shear gradient, respectively. Still, using P_1-4 as an example, we present parts b and c of Figure 5, the 2D WAXD patterns recorded at room temperatures with the X-ray incident beam parallel to *z*- and *y*-direction, respectively. We also tried to obtain the diffraction pattern with the incident beam parallel to the shear direction, but found the diffractions were not clear enough. In both Figures 5b and 5c with the shear direction along the meridian, all the low-angle diffractions appear on the equator. On the other hand, a pair of the high-angle diffractions, which is mainly resulted from the interference of side-chains which pack parallel to each other, is located on the meridian in Figure 5b. Considering that the strong mechanical shearing can preferentially align the main-chain axis parallel to the shear direction, this geometry of high-angle diffraction signifies that the side-chains are perpendicular to the main-chain axis. Interestingly, as shown in Figure 5c, when the X-ray incident beam is aligned parallel to *y*-direction, we observe that the high-angle diffraction can also appear in the quadrants in addition to that shown on the meridian. Because it

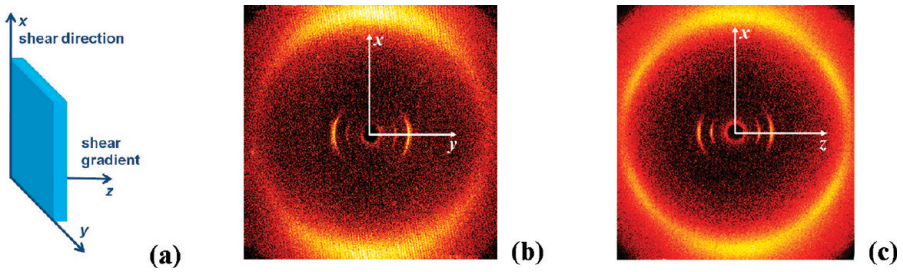

Figure 5. (a) Schematic drawing of the sheared sample with x and z direction the shear direction and shear gradient, respectively. (b and c), 2D WAXD patterns of P_1-4 at room temperature with the shear direction on the meridian. The X-ray incident beam is directed along the (b) z- and (c) y-directions, respectively.

involves the scattering from the repeating units along the main-chains, the pair of arcs on the meridian is more intense and broader than the others. The six diffraction arcs at 2θ of 20.3° in fact possess a 6-fold symmetry. The corresponding azimuthal intensity profile confirmed that the angle between two adjacent diffraction maxima is 60°. Consequently, we conclude that at low temperatures the side-chains form a SmB-like packing, which is seldom found in azobenzene containing LC polymers, with a of the hexagonal lattice (denoted as a' below) of 0.51 nm. It is worthy to mention here that the 6-fold symmetry of side-chain pack is not observed in Figure 5b, which implies that the ordered domains within the sample are not completely rotationally disordered around the shear direction. Likely, the side-chain axis within the sheared film is not only perpendicular to the main-chain axis along the shear direction but also preferentially parallel to the y-direction. In this case, the sheared sample probably possesses a macroscopically biaxial orientation.

With the main-chain along the meridian, the low-angle diffractions located on the equator can be assigned as ($hk0$) of the main-chain ordered packing. Note that in 1D WAXD patterns the two diffractions of 2 and 3 which are very close to each other are weaker than that of diffraction 1 at low temperatures (see Figure 4). However, in the 2D WAXD patterns the diffractions located at the same 2θ angles of 2 and 3 become rather intense, implying that the orientation due to shearing can greatly enhance these diffractions. This diffraction behavior is reminiscent of that of some azobenzene containing SCLCPs with interdigitated SmA phase (also see below),[52,54] suggesting that either diffraction 2 or diffraction 3 would be related to the layer structure determined by the side-chain packing. Since only a few pairs of diffractions are recognized, we tentatively presume that P_1 can form a 2D centered rectangular lattice with its a-axis along the side-chain direction, analogous to that found in PBBHCS. We may assign 3 to be (400) diffraction, and 1 and 4 to be (110) and (220) diffraction, respectively. This indexing leads to a rectangular lattice with a = 4.84 nm and b = 2.14 nm at 30 °C. In this case, the calculated d-spacing of (310) is 1.29 nm, almost identical to the measured d-spacing of peak 2. Therefore, the indexing looks reasonable. Taking the values of a and b at 30 °C and assuming the projection length of two repeating units on the main-chain to be ~0.42 nm,[37,39] the density of P_1 can be estimated to be ~1.07 g/cm^3, in good agreement with the measured value of 1.06 g/cm^3 at room temperature.

The possible supramolecular structure of P_1 at low temperatures is schematically drawn in Figure 6, which can be used to explain our experimental observations. Figure 6a illustrates the lattice viewed along the main-chain axis. It is intriguing to note

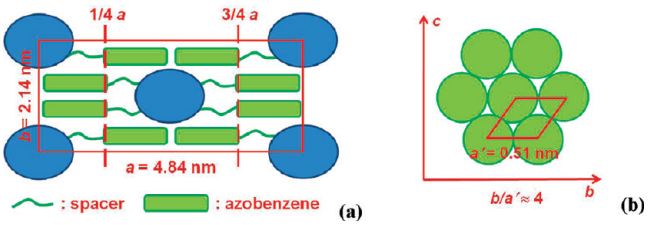

Figure 6. Schematic drawing of the proposed supramolecular structure for P_1 at low temperatures and view along the main-chain (a) and side-chain (b) directions, respectively.

that the length of p-methoxyazobenzene in P_1 (l_{azo}) is of ~1.2 nm, and thus the ratio of a/l_{azo} is of ~4. We consider that the side-chains emanating from the same main-chain can extend to two opposite directions parallel to a-axis, which fully interdigitated pack with the side-chains from the adjacent chain molecules.[54−56] In this case, the densities at one-fourth and third fourth of the a-axis (see the dashed lines indexed in Figure 6a) might closely match to that of the position occupied by the main-chains.[54] This could be a reason to account for the missing of (200) diffraction of P_1 and the low intensity of (400) diffraction. On the other hand, the side-chain length of 5.5 nm calculated with the assumption of the all-trans conformation for the methylene units is obviously longer than the value of a. Therefore, we presume that the flexible spacers of the side-chain adopt many gauche conformations when the side-chains fill the space within the main-chain scaffold. Figure 6b shows the molecular packing viewed along the side-chain direction. According to high-angle diffraction geometry shown in Figure 5c, a'-axis of the SmB-like structure of side-chain shall be perpendicular to the main-chain axis (c-axis) and collinear with b-axis of the main-chain scaffold. Note that $b/a' \approx 4$, suggesting that the 2D rectangular lattice includes eight subunit cells of the SmB-like structure.[57,58]

Figure 4 shows that the four low-angle diffractions remain until the temperature exceeds the highest transition temperature. We find that the indexing of the peaks suggested above, e.g., 1 the (110), 2 the (310), 3 the (400), and 4 the (220), can be well applied to the 1D WAXD patterns recorded at different temperatures, indicating the main-chain scaffold does not vary its symmetry upon heating. This observation was confirmed by 2D WAXD experiments. Parts a and b of Figure 7 describe 2D WAXD patterns of the sheared P_1-4 sample at 140 and 165 °C, respectively, with the X-ray incident beam parallel to the z-direction. Compared to Figure 5b recorded at room temperature, Figure 7a shows that the low-angle equatorial diffractions looks

unchanged. Meanwhile, the scattering concentrated on the meridian becomes much more diffuse. At 165 °C, a diffuse ring appears in the high-angle region, but the equatorial diffractions with lowered intensities can still be recognized. Further heating to above the highest transition temperature, the main-chain diffraction of P_1 completely lost. This situation is different from that of PBBHCS which has a conventional SmA phase after the main-chain scaffold melting.

While the main-chain scaffold sustains until the isotropic transition, the low- and middle-temperature transitions of P_1 shall be tightly associated with the change of side-chain packing. On the basis of the high-angle diffraction/scattering shown in Figure 4, we plot in Figure 8a the *d*-spacing corresponding to the peak position and the full-width of half-height (fwhh) as functions of temperature, wherein the dashed vertical lines index the transition temperatures detected by DSC. In addition, Figure 8b illustrates the temperature dependence of the calculated *a* and *b* of the supramolecular lattice. When the relatively shape high-angle diffraction turns into a broad scattering halo at ~110 °C (see Figure 4), the *d*-spacing and fwhh jump to higher values in Figure 8a, indicating that the low-temperature transition is the melting of SmB-like structure. This transition causes a significant expansion of *b* (see Figure 8b), inferring that the packing of azobenzene side-chain becomes loose. Considering that the main-chain scaffold in fact provide a sort of layer-like structure for the side-chain packing, we suggest that within the temperature range of 110−160 °C the side-chains possess a SmA-like packing. When temperature approaches 160 °C, the *d*-spacing and fwhh in Figure 8a present again discontinuous increases, accompanying with a rise in the *a* dimension (see Figure 8b). As evidenced in Figure 7b, the side-chains lose their orientation in the high temperature range. Therefore, the side-chain packing becomes largely isotropic. On the basis of all the experimental results, we propose that the sequence of phase transitions of P_1 follows: isotropic ↔ 2D centered rectangular scaffold of main-chain and isotropic side-chain ↔ 2D centered rectangular scaffold of main-chain and SmA-like structure of side-chain ↔ 2D centered rectangular scaffold of main-chain and SmB-like structure of side-chain.

Comparison between P_1 and P_2. According to the chemical structure shown in Chart 1, P_2 is a conventional SCLCP with the mesogenic groups terminally attached to the main-chain via a flexible spacer. Figure 9 describes a set of DSC cooling and subsequent heating diagrams of P_2 at different rates (2.5−20 °C/min), wherein two transitions can be identified. The cooling curve shows that a broad and relatively weak exothermic process follows immediately the sharp one with the onset temperature of 122 °C. Upon heating, the two transitions are largely overlapped. Previously, we studied the molecular packing and phase transitions of a series of SCLC polymethacrylates with *p*-methoxyazobenzene group linked to the backbone through a flexible spacer (PM*n*Az, *n* is the methylene unit number of spacer, *n* = 6−12).[54] The phase

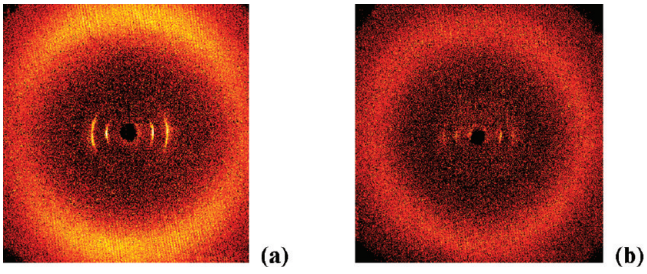

Figure 7. 2D WAXD patterns of the sheared P_1-4 sample recorded at (a) 140 and (b) 165 °C. The shear direction is on the meridian and the X-ray incident beam is along the *z*-direction.

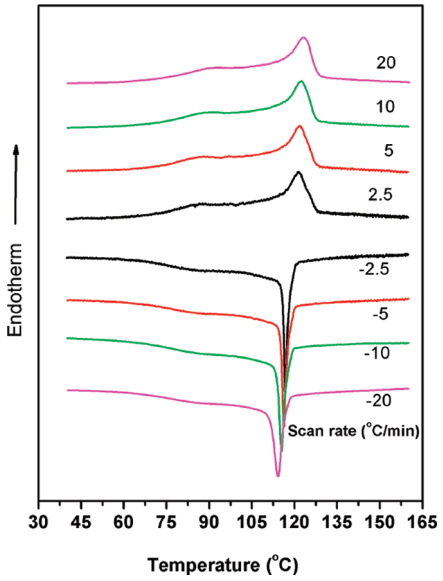

Figure 9. DSC curves of cooling and subsequent heating of P_2 at different rates.

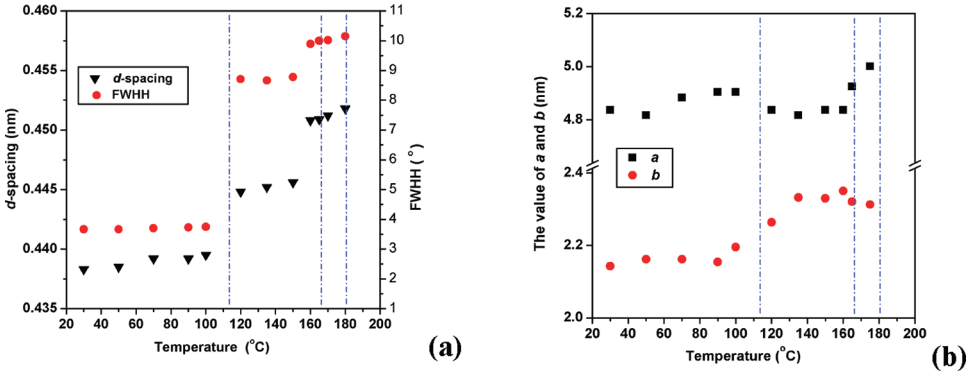

Figure 8. (a) *d*-spacing at the peak position and full width of half-height (fwhh) of the high-angle diffraction/scattering as functions of temperature. The data plotted are obtained from Figure 4 of P_1-4. (b) Temperature dependence of the calculated *a* and *b* of the rectangular lattice of P_1-4.

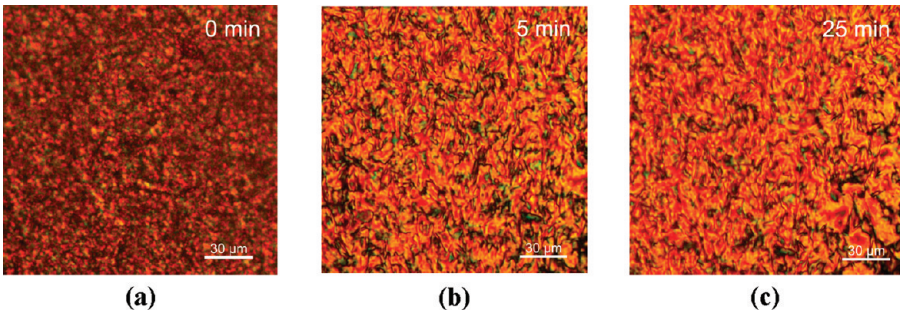

Figure 10. POM images of P_1 recorded at 80 °C under UV irradiation. The exposal times are (a) 0, (b) 5, and (c) 25 min, respectively.

transition of PM*n*Az follows the sequence of isotopic ↔ N ↔ SmA. The PM*n*Az samples with relatively long spacers ($n = 10, 12$) also possess two transition temperatures very close to each other, of which the thermal behavior is quite similar to that of P_2. Considering the chemical structure of P_2 is similar to that of PM*n*Az despite the difference in backbones, we consider that P_2 can share with PM*n*Az the same phase transition behavior. The solution casting sample and the sample cooled from the isotropic state of P_2 could not provide clear diffractions, but their POM texture unambiguously indicated the LC phases (see the Supporting Information). This situation was encountered in the PM*n*Az samples.[54] Nevertheless, the diffractions featuring the SmA structure could be detected from orientated P_2 samples (see the Supporting Information). The first-order diffraction in the low-angle region corresponded to a *d*-spacing of 3.20 nm, slightly larger than the side-chain length of 3.02 nm estimated with an assumption that the alkyl spacer adopts an all-trans conformation. Therefore, P_2 formed a monolayer SmA phase at low temperatures, with an almost fully interdigitated packing of the side-chains from two adjacent sublayers of the main-chains.

In comparison with P_1 that can form a highly ordered LC phase composed of the main-chain rectangular scaffold and SmB-like packing of side-chains, P_2 exhibits simpler and lower ordered LC phases. In the SmA structure, the P_2 backbones should be located in the sublayers separated by the adjacent side-chain sublayers. The poly[(4-oxycarbonyl)styrene] backbone of P_2, which is semirigid, is "invisible" in X-ray diffraction experiments due to the lack of positional order. It is quite possible that the backbone conformation of P_2 is squeezed to be an oblate random coil, but not rod-like. It is interesting to compare the transition temperatures of P_1 with that of P_2. For P_2, the endothermic process ends at ∼130 °C, significantly lower than the temperature of SmA-like structure melting of P_1. We should consider that the main-chain scaffold of P_1 in fact imposes confinement on the side-chains, which can stabilize the SmA-like packing. Moreover, such a confinement can even induce the SmB-like packing of the side-chains at low temperatures, which is hardly achieved in conventional SCLC polymers containing azobenzene mesogens. This confinement effect has a MW dependent. As shown in Figure 2b, the transition temperatures of P_1 increase with increasing MW. The longer the P_1 chain is, the more stable 2D centered rectangular lattice forms, and the expansions of *a* and *b* become more difficult. Consequently, the SmB- and SmA-like structure melting, which are associated with the increasing of *b* and *a* dimension (see Figure 8), respectively, occur at higher temperatures when MW is increased.

It is well-known that azobenzene chromophore can undergo reversible trans−cis isomerization under photoirradiation. When exposed to UV irradiation ($\lambda = 365$ nm) at low temperatures, P_2 thin films would lose birefringence under POM, indicating that the sample could completely become isotropic. This photoinduced phase transition is the same as that observed in other azobenzene containing SCLCPs,[59,60] which is due to that the azobenzene group adopts cis conformation. However, P_1 behaved different. Figure 10 shows the POM images of a P_1 thin film sequentially recorded under UV irradiation at 80 °C. Obviously, the original grainy texture (Figure 10a) is changed to be a typical schlieren texture (Figure 10b) after the sample was exposed to the irradiation. With increasing the exposal time, the schlieren texture remains as shown in Figure 10c. This observation indicates that UV irradiation cannot lead to an isotropic state of P_1. The two and four brushes appeared in Figures 10b and 10c imply a N phase. Note that under UV irradiation the azobenzene group with cis conformation is no longer a mesogen. Therefore, the survived LC structure should be attributed to the existence of rod-like main-chains of P_1 which are little affected by the UV irradiation. Tentatively, we presume that the UV-induced phase could be Φ_N.[37]

CONCLUSION

Aiming to synthesize MCSCLCP based on chain polymerization method, we have explored the molecular design based on the combination of "flexible spacer" concept and side-group "jacketing" effect. While the "flexible spacer" can be used to bring mesogenic groups to the side-chains, the side-group "jacketing" effect can make the main-chain rod-like. We successfully synthesized a new MCSCLCP based on radical polymerization of 2-vinylterephthalate monomer containing two azobenzene groups (P_1). In addition to our previous study on a similar polymer with biphenyl mesogens (PBBHCS), we demonstrate here that our molecular design of MCSCLCP can apply to various rod-like mesogens. We identify that P_1 can form a hierarchically ordered structure with double orderings on nanometer and subnanometer length scales, respectively. The "jacketing" effect results in a main-chain of P_1 composed of the polyethylene backbone and the central rigid portion of terephthalate side-chain. Most likely, the thick main-chains construct a 2D centered rectangular scaffold, which is stable until the sample enters a completely isotropic state. The azobenzene containing side-chains pack inside the main-chain scaffold, with their direction perpendicular to the main-chain at low temperatures. The observed SmB-like structure of side-chain packing at below the lowest transition temperature of P_1 is unexpected, which shall be due to the confinement imposed by the main-chain scaffold that can force the azobenzen groups to pack closer.

Upon heating, the SmB-like packing of side-chains transforms into a SmA-like structure followed by a transition of SmA-to-isotropic. We also observe that the confinement effect can greatly enhance the thermal stability of the SmA-like packing of azobenzene moiety. We compare the phase behaviors between P_1 and a conventional SCLCP (P_2) with one azobenzene group per repeating unit. P_2 just form a monolayer SmA phase at low temperatures, and its transition temperatures are much lower than that of P_1. This comparison verifies that the main-chain scaffold confinement effect is important for the azobenzene side-chain packing in P_1. As P_1 exhibit a fascinating hierarchical ordering, we are also interested in investigating how the supramolecular structure will influence the photoresponsive behavior of azobenzene group or vice versa. Our preliminary result shows that P_1 remains its LC property under UV irradiation, in contrast to that P_2 can become completely isotropic. The UV-induced LC phase of P_1 might be a Φ_N phase, reflecting the existence of rod-like main-chains. More researches on the photoinduced anisotropy and photochemical phase transition of P_1 are ongoing and will be reported later.

■ ASSOCIATED CONTENT

Ⓢ Supporting Information. Materials and experimental details, and figures showing GPC curves of P_1 with different MWs, ^{1}H NMR spectra of M_2 and P_2, POM images of P_2, and 1D and 2D WAXD patterns of P_2. This material is available free of charge via the Internet at http://pubs.acs.org.

■ AUTHOR INFORMATION

Corresponding Author

*E-mail: hailiangzhang@xtu.edu.cn (H.-L.Z.); eqchen@pku.edu.cn (E.-Q.C.).

■ ACKNOWLEDGMENT

This work is supported by the National Natural Science Foundation of China (NNSFC Grants: 20874082, 20990232, 21074003, and 51073131), the Natural Science Foundation of Xiangtan University (No: 10XZX09) and Hunan Provincial Natural Science Foundation of China (No: 11JJ4012).

■ REFERENCES

(1) Blumstein, A. *Polymeric Liquid Crystals*; Plenum Press: New York, 1985.
(2) Mcardle, C. B. *Side Chain Liquid Crystal Polymers*; Blackie and Son Ltd: Glasgow, U.K., 1989.
(3) Percec, V.; Pugh, C. *Side Chain Liquid Crystal Polymers*; MacArdle, C. B., Ed: Blackie: Glasgow, U.K., 1989.
(4) Simmonds, D. J. *Liquid Crystal Polymers, From Structures to Applications*; Elsevier Applied Science: London and New York, 1992.
(5) Mao, G.; Ober, C. K. *Acta Polym.* **1997**, *48*, 405–422.
(6) Maughon, B. R.; Weck, M.; Mohr, B.; Grubbs, R. H. *Macromolecules* **1997**, *30*, 257–265.
(7) Nieuwhof, R. P.; Koudijs, A.; Marcelis, A. T. M.; Sudhölter, E. J. R. *Macromolecules* **1999**, *32*, 6499–6506.
(8) Percec, V.; Tomazos, D.; Willingham, R. A. *Polym. Bull.* **1989**, *22*, 199–206.
(9) Ranganathan, T.; Bhoje Gowd, E.; Ramesh, C.; Kumar, A. *J. Polym. Sci. Part A: Polym. Chem* **2005**, *43*, 1903–1912.
(10) Watanabe, J.; Ono, H.; Uematsu, I.; Abe, A. *Macromolecules* **1985**, *18*, 2141–2148.
(11) Jin, S.; Jeong, K. U.; Tu, Y.; Graham, M. J.; Wang, J.; Harris, F. W.; Cheng, S. Z. D. *Macromolecules* **2007**, *40*, 5450–5459.
(12) Zentel, R.; Brehmer, M. *Acta Polym.* **1996**, *47*, 141–149.
(13) Reck, B.; Ringsdorf, H. *Makromol. Chem.* **1985**, *6*, 291–299.
(14) Reck, B.; Ringsdorf, H. *Makromol. Chem.* **1986**, *7*, 389–396.
(15) Cooray, N. F.; Fujimoto, H.; Kakimoto, M.-a.; Imai, Y. *Macromolecules* **1997**, *30*, 3169–3174.
(16) Ge, J. J.; Zhang, A. Q.; McCreight, K. W.; Ho, R. M.; Wang, S. Y.; Jin, X. M.; Harris, F. W.; Cheng, S. Z. D. *Macromolecules* **1997**, *30*, 6498–6506.
(17) Huang, W.; Han, C. D. *Macromolecules* **2006**, *39*, 4735–4745.
(18) Joo, S.-H.; Yun, Y.-K.; Jin, J.-I.; Kim, D.-C.; Zin, W.-C. *Macromolecules* **2000**, *33*, 6704–6712.
(19) Lam, J. W. Y.; Tang, B. Z. *Acc. Chem. Res.* **2005**, *38*, 745–754.
(20) Piao, X. L.; Kim, J.-S.; Yun, Y.-K.; Jin, J.-I.; Hong, S.-K. *Macromolecules* **1997**, *30*, 2294–2299.
(21) Ruan, J. J.; Jin, S.; Ge, J. J.; Jeong, K. U.; Graham, M. J.; Zhang, D.; Harris, F. W.; Lotz, B.; Cheng, S. Z. D. *Polymer* **2006**, *47*, 4182–4193.
(22) Schaefer, K. E.; Keller, P.; Deming, T. J. *Macromolecules* **2006**, *39*, 19–22.
(23) Zhou, M.; Han, C. D. *Macromolecules* **2005**, *38*, 9602–9609.
(24) Xie, H.; Hu, T.; Zhang, X.; Zhang, H.; Chen, E.; Zhou, Q. *J. Polym. Sci. Part A: Polym. Chem* **2008**, *46*, 7310–7340.
(25) Chen, X.-F.; Shen, Z.; Wan, X.-H.; Fan, X.-H.; Chen, E.-Q.; Ma, Y.; Zhou, Q.-F. *Chem. Soc. Rev.* **2010**, *39*, 3072–3101.
(26) Zhou, Q. F.; Li, H. M.; Feng, X. D. *Macromolecules* **1987**, *20*, 233–234.
(27) Zhou, Q. F.; Zhu, X. L.; Wen, Z. Q. *Macromolecules* **1989**, *22*, 491–493.
(28) Chen, X. F.; Tenneti, K. K.; Li, C. Y.; Bai, Y. W.; Zhou, R.; Wan, X. H.; Fan, X. H.; Zhou, Q. F. *Macromolecules* **2006**, *39*, 517–527.
(29) Gopalan, P.; Andruzzi, L.; Li, X.; Ober, C. K. *Macromol. Chem. Phys.* **2002**, *203*, 1573–1583.
(30) Gray, G. W.; Hill, J. S.; Lacey, D. *Mol. Cryst. Liq. Cryst.* **1991**, *197*, 43–55.
(31) Hessel, F.; Herr, R. P.; Finkelmann, H. *Makromol. Chem.* **1987**, *188*, 1597–1611.
(32) Keller, P.; Hardouin, R.; Mauzac, M.; Achard, M. *Mol. Cryst. Liq. Cryst.* **1998**, *155*, 71–80.
(33) Percec, V.; Tomazos, D. *J. Matter. Chem.* **1993**, *3*, 643–650.
(34) Pragliola, S.; Ober, C. K.; Mather, P. T.; Jeon, H. G. *Macromol. Chem. Phys.* **1999**, *200*, 2338–2344.
(35) Pugh, C.; Schrock, R. R. *Macromolecules* **1992**, *25*, 6593–6604.
(36) Xu, Y.; Yang, Q.; Shen, Z.; Chen, X.; Fan, X.; Zhou, Q. *Macromolecules* **2009**, *42*, 2542–2550.
(37) Ye, C.; Zhang, H. L.; Huang, Y.; Chen, E. Q.; Lu, Y. L.; Shen, D. Y.; Wan, X. H.; Shen, Z. H.; Cheng, S. Z. D.; Zhou, Q. F. *Macromolecules* **2004**, *37*, 7188–7196.
(38) Yin, X. Y.; Ye, C.; Ma, X.; Chen, E. Q.; Qi, X. Y.; Duan, X. F.; Wan, X. H.; Cheng, S. Z. D.; Zhou, Q. F. *J. Am. Chem. Soc.* **2003**, *125*, 6854–6855.
(39) Xie, H. L.; Jie, C. K.; Yu, Z. Q.; Liu, X. B.; Zhang, H. L.; Shen, Z. H.; Chen, E. Q.; Zhou, Q. F. *J. Am. Chem. Soc.* **2010**, *132*, 8071–8080.
(40) Cojocariu, C.; Rochon, P. *Macromolecules* **2005**, *38*, 9526–9538.
(41) Freiberg, S.; Lagugne-Labarthet, F.; Rochon, P.; Natansohn, A. *Macromolecules* **2003**, *36*, 2680–2688.
(42) Li, M. H.; Auroy, P.; Keller, P. *Liq. Cryst.* **2000**, *27*, 1497–1502.
(43) Mao, G. P.; Wang, J. G.; Clingman, S. R.; Ober, C. K.; Chen, J. T.; Thomas, E. L. *Macromolecules* **1997**, *30*, 2556–2567.
(44) Wolff, D.; Cackovic, H.; Kruger, H.; Rubner, J.; Springer, J. *Liq. Cryst.* **1993**, *14*, 917–928.
(45) Del Barrio, J.; Oriol, L.; Sanchez, C.; Serrano, J. L.; Di Cicco, A.; Keller, P.; Li, M. H. *J. Am. Chem. Soc.* **2010**, *132*, 3762–3769.
(46) Deng, W.; Albouy, P. A.; Lacaze, E.; Keller, P.; Wang, X. G.; Li, M. H. *Macromolecules* **2008**, *41*, 2459–2466.
(47) Deng, W.; Li, M. H.; Wang, X. G.; Keller, P. *Liq. Cryst.* **2009**, *36*, 1023–1029.
(48) Yu, Y. L.; Ikeda, T. *Angew. Chem. Int. Ed* **2006**, *45*, 5416–5418.

(49) Han, D.; Tong, X.; Zhao, Y. *Macromolecules* **2011**, *44*, 437–439.
(50) Han, D. H.; Tong, X.; Zhao, Y.; Galstian, T.; Zhao, Y. *Macromolecules* **2010**, *43*, 3664–3671.
(51) Ikeda, T.; Mamiya, J.; Yu, Y. L. *Angew. Chem. Int. Ed* **2007**, *46*, 506–528.
(52) Natansohn, A.; Rochon, P. *Chem. Rev.* **2002**, *102*, 4139–4175.
(53) Matyjaszewski, K.; Xia, J. H. *Chem. Rev.* **2001**, *101*, 2921–2990.
(54) Zhu, X. Q.; Liu, J. H.; Liu, Y. X.; Chen, E. Q. *Polymer* **2008**, *49*, 3103–3110.
(55) Watanabe, J.; Ono, H.; Uematsu, I.; Abe, A. *Macromolecules* **1985**, *18*, 2141–2148.
(56) Watanabe, J.; Tominaga, T. *Macromolecules* **1993**, *26*, 4032–4036.
(57) Demus, D.; Goodby, J.; Gray, G. W. *Handbook of Liquid Crystals*; WILEY-VCH: Weinheim, 1998.
(58) Gray, G. W.; Vill, V., Spiess; H.W., D.; Goodby, J. W. *Physical Properties of Liquid Crystals*; WILEY-VCH: Weinheim, Germany, 1999.
(59) Ikeda, T.; Tsutsumi, O. *Science* **1995**, *268*, 1873–1875.
(60) Ikeda, T.; Shiono, T.; Tsutsumi, O.; Galli, G. *J. Phys. Chem. B* **1997**, *101*, 1332–1337.